



# Facile synthesis of petal-like NiCo/NiO-CoO/nanoporous carbon composite based on mixed-metallic MOFs and their application for electrocatalytic oxidation of methanol

Sharifeh Rezaee<sup>a</sup>, Saeed Shahrokhian<sup>a,b,\*</sup>

<sup>a</sup> Department of Chemistry, Sharif University of Technology, Tehran, 11155–9516, Iran

<sup>b</sup> Institute for Nanoscience and Technology, Sharif University of Technology, Tehran, Iran

## ARTICLE INFO

### Keywords:

Metal-organic  
Framework  
Non-precious catalyst  
Mixed transition metal oxides  
Electrocatalytic oxidation  
Multi-component composites

## ABSTRACT

Porous carbon template decorated with mixed transition metals/metal oxides with tunable architecture is becoming increasingly important and attractive as a kind of novel electrode materials. In this way, mixed-metallic metal-organic frameworks (MOFs) provide an opportunity for fabrication of homogeneous mixed metals/metal oxides distribution in the porous carbon frame without any carbon precursor additive. Also, structures, dimensions and electrochemical performance of MOFs can be readily manipulated by simply tuning the metals molar ratio. In this study, we demonstrate the design and fabrication of petal-like NiCo/NiO-CoO metal/metal oxides with a rational composition embedded in 3D ultrathin nanoporous carbon composite (NiCo/NiO-CoO/NPCC). This nanocomposite is synthesized by a two-steps procedure involving preparation of bimetallic MOFs by partially substituting  $\text{Ni}^{2+}$  in the Ni-MOF structure with  $\text{Co}^{2+}$  (Ni-Co/BDC [BDC = 1,4-Benzenedicarboxylic acid]) and direct carbonization process in the  $\text{N}_2$  atmosphere at 900 °C. The prepared nanocomposite was used directly as a non-precious electrocatalyst for methanol oxidation reaction. The results indicated that, in comparison to the monometallic metal/metal oxides distributed in nanoporous carbon composite (Ni/NiO/NPCC and Co/CoO/NPCC), the mixed metals/metal oxides NiCo/NiO-CoO/NPCC exhibits excellent electrochemical performance toward the anodic oxidation of methanol. The unique ultrathin porous petal-like structure with free pores and the enlarged specific surface area provides fast ion/electron transfer, leading to faster kinetics, lower over-potential, and higher electro-catalytic reactivity. Besides their intriguing structural features, the excellent conductivity of carbon frame, as well as a rational composition of two constituents and synergistic effects from cobalt, nickel and their oxides provides favorable catalytic activity for the electro-oxidation of methanol. Therefore, it is believed that this novel multi-component composites demonstrates good electrocatalytic activity and suitable stability towards the methanol oxidation.

## 1. Introduction

Direct methanol fuel cell (DMFCs), as an attractive and promising power source for future energy demand, has attracted a great deal of attention because of its simplicity, potentially renewable fuel and high theoretical efficiency of the energy conversion [1]. Nevertheless, slow kinetics of the methanol oxidation reaction at the anode electrodes, which leads to large over-voltages, is one of the major challenges toward the commercialization of DMFCs [2]. Although noble metals and their alloys with effective catalytic role exhibit high electro-catalytic activities, however, great price and scarcity of the metals may restrict their commercial applications. Therefore, discovering low-cost and novel anode electrocatalysts is highly desirable and important. Lately, a

great deal of effort was devoted to developing transition metals oxides as proper substitutes for the noble metals catalysts [3]. Thus, substantial researches have been centered on the use of transition metal oxides catalysts such as NiO [4], CoO [5] and  $\text{Cu}_2\text{O}$  [6] for DMFCs, because of their low production cost, commercial availability and high electrocatalytic activity.

Also it worth to note that, formulation of composites is a fascinating strategy for increase the electro-catalytic performances, robustness and engagement ability of the catalysts [7]. Generally, multi-component catalysts, due to synergistic advantages, exhibit novel properties beyond each individual component through the reinforcement or modification of each other [8]. Thus, exploring novel mixed transition metal/metal oxides with the rational design of multi-component

\* Corresponding author at: Department of Chemistry, Sharif University of Technology, Tehran, 11155–9516, Iran.

E-mail address: [shahrokhian@sharif.edu](mailto:shahrokhian@sharif.edu) (S. Shahrokhian).

<https://doi.org/10.1016/j.apcatb.2018.12.013>

Received 4 September 2018; Received in revised form 16 November 2018; Accepted 3 December 2018

Available online 05 December 2018

0926-3373/ © 2018 Elsevier B.V. All rights reserved.

combination has become an important research direction. The obtained results indicate that creation of a link between metals rendering the mixed transition metal/metal oxides rich in redox reactions [9]. Till now, there have been some reports on the application of multi-component catalysts containing transition metal and metal oxides in the electro-oxidation reactions. For example, Liu et al. [10] fabricated a nanocomposite of CoO–NiO–NiCo supported by nitrogen-doped multi-wall carbon nanotubes as a bifunctional electrocatalyst for the oxygen reduction reaction and also the oxygen evolution reaction. Wu et al. [11] prepared NiCo/NiO–CoOx ultrathin layered nanocomposites as a non-noble-metal multifunctional catalyst for catalyzing H<sub>2</sub> generation from N<sub>2</sub>H<sub>4</sub>. Also, Peng et al. [12] prepared a homologous Ni–Co based nanowire system consisting of both nickel cobalt oxide and Ni<sub>0.33</sub>Co<sub>0.67</sub>S<sub>2</sub> nanowires for efficient, complementary water splitting. Moreover, Zhang et al. prepared Ni–Co bimetallic MgO-based catalysts for hydrogen production via steam reforming of acetic acid from bio-oil [13]. Therefore, based on the above-mentioned work, multi-component catalysts such as NiCo/NiO–CoO can meet the requirements for designing high-performance catalysts for direct electro-oxidation of methanol.

It should be noted that, metal oxides suffer from poor electric conductivity and this problem can be compensated by synthesis the composites of them with a typical carbon-based material such as carbon fiber [14], carbon hollow particles [15], carbon nanoflakes [16] graphene [17] and carbon nanotubes [18]. Hence, it is believed that synthesis of composites containing conductive nanocarbon materials is an effective strategy to improving catalytic activity, through increasing number of available active sites and providing efficient charge transport channels. As promising candidate nanoporous carbon materials with high surface areas, narrow pore size distribution, high pore volume, and high conductivity can be considered as a suitable support for preparation of electrocatalysts. Besides the composition, the morphology, shape, and structural characteristics are other crucial approaches to efficient control of the catalytic activity of catalysts, which is attributed to the structure-activity relationships [19]. In this regard, petal-like structures assembled by interconnected two-dimensional nanosheets with porous structures are greatly desirable and can be considered as the nanostructures with efficient catalytic properties. The obtained results revealed that these materials are favorable to efficient ion and electron transport and fast reaction kinetics, due to their large surface area, high catalytic activity, high roughness, high porosity and sufficient adsorption sites for a specific electrochemical reaction [20].

The most widely used method for the preparation of nanocomposites containing metal/metal oxides and carbon nanomaterials is based on dispersing the metal components into the carbon support. As a point that should be noted, heterogeneous catalysts often suffer from particles aggregation during the reaction progress and thus resulting loss in their catalytic activity [21]. Therefore, we need to find a simple and facile route for the synthesis of the seamless nanocomposites, in order to effective immobilization of metal oxide nanoparticles with high stability and fine distribution on porous carbon supports.

As an appropriate candidate, metal-organic frameworks (MOF) a new class of porous materials assembled by metal-containing units and bridging organic ligands have attracted immense attentions [22]. MOFs present various superior properties, such as porous structure, high surface area, and diverse structural topology. Hence, MOFs can use in many applications in electrochemical energy storage, including hydrogen production and storage, fuel cells, lithium-ion batteries, supercapacitors and solar cells [23]. However, the poor conductivity and unstable nature of MOFs in aqueous solutions limited their application. Therefore, according to the conditions of usage, MOFs can be used as precursors or templates for preparation of nano-sized materials such as porous carbon, metals, metal oxides, and hydroxides [24]. Accordingly, mixed-metal MOFs are used for the preparation of highly porous carbon materials and hybrid meta/metal oxides via direct carbonization. As a result, the metal compositions can be converted into metallic or metal

oxide nanoparticles while organic ligand can be transformed into porous carbon materials. Also, during the carbonization process, the primary morphology of MOFs is retained. Mixed-metal MOFs are composed of two different central metal ions into a same framework with a further degree of structural stability and conductivity [25]. Because of the similar ion radius of Co and Ni, partial substitution of nickel cations with cobalt can be occurring without serious changing in the crystalline structure of Ni-MOF. Then, mixed Ni/Co nanoparticles and NiO/CoO metal oxides distributed in the carbon frame can be prepared after the direct carbonization of bimetallic Ni–Co/MOF. In comparison to other methods, synthesis of metal/metal oxides/porous carbon nanocomposites from the corresponding MOFs has noticeable benefits. In one hand, the wide variety of MOFs makes it possible to achieve more pure metal/metal oxides with different components and homogeneous distribution. On the other hand, the obtained nanocomposites from MOFs have diverse shapes and structures with high surface area, which make them desirable as the electrocatalyst for the electro-oxidation reactions. Recently, some research groups have suggested different catalysts based on MOFs. For example, Raoof et al. [26] prepared MOF-derived Cu/nanoporous carbon composite as a non-platinum electrocatalyst for the hydrogen evolution reaction. Also, Peng, et al prepared Ni/Co bimetallic metal–organic framework nanobelts as an excellent bifunctional oxygen catalyst [27]. Pang et al. reported the fabrication of Ni/NiO/carbon frame nanocomposite from nickel-based MOFs and investigated as a nonenzymatic glucose and H<sub>2</sub>O<sub>2</sub> sensors [28]. Also in another work synthesized ultrathin two-dimensional cobalt–organic framework nanosheets by a simple surfactant-assisted hydrothermal method for high-performance electrocatalytic oxygen evolution reaction [29].

Ali Khan et al. synthesized the nanoporous carbon by direct carbonization of MOF-5 and studied it as a support for the preparation of an electrocatalyst for the electro-oxidation of ethanol [30].

Based on the above considerations, the aim of this study is to develop noble metal-free electrocatalysts for DMFCs. Therefore, in this study we present a simple method to synthesize mixed NiCo/NiO–CoO/nanoporous carbon composite (NiCo/NiO–CoO/NPCC) with a petal-like structure. For this purpose, we have used bimetallic Ni–Co/MOF as the precursor template for the fabrication of nanocomposites containing mixed metal/metal oxide/carbon frame by direct carbonization without any carbon precursors. This process finally yielded stable composites with ultrafine distribution of metal/metal oxide nanoparticles in the carbon support. The obtained nanocomposites have large surface area, high pore volume, and high chemical stability with an easy synthesis procedure. The electro-oxidation of methanol on NiCo/NiO–CoO/NPCC has been studied by different electrochemical techniques. The obtained results reveal that, in comparison to simple Ni/NiO or Co/CoO, the mixed metal/metal oxide with unique porous structure and strong synergistic effect from Ni, Co, NiO and CoO shows a noticeable catalytic activity. To the best of our knowledge, this is the first report on the synthesis of the NiCo/NiO–CoO/NPCC nanocomposite from bimetallic MOFs and its application for use in direct methanol oxidation.

## 2. Experimental section

### 2.1. Materials and instrumentation

Cobalt (II) nitrate hexahydrate (Co(NO<sub>3</sub>)<sub>2</sub>·6H<sub>2</sub>O), Nickel (II) chloride (NiCl<sub>2</sub>), N,N-dimethylformamide (DMF), sodium hydroxide, ethanol, and methanol EITH analytical reagent grade were purchased from Merck. 1,4-Benzene dicarboxylic acid (H<sub>2</sub>BDC, 95%) was obtained from Aldrich. The reagents used for electrochemical impedance studies, including K<sub>3</sub>Fe(CN)<sub>6</sub>, K<sub>4</sub>Fe(CN)<sub>6</sub> and KCl (> 99%), were also prepared from Merck. All aqueous solutions were prepared using ultra-pure deionized water (18.2 MΩ, Zolalan Sharif Company, Tehran, Iran).



Scheme 1. Schematic illustration of the synthetic process of NiCo/NiO-CoO/NPCC.

## 2.2. Instrumentation

The electrochemical experiments were performed using a potentiostat/galvanostat from Sama Instrument (500-C Electrochemical analysis system, Sama, Iran) coupled with a PC through an interface with Sama-500 software version 2.7. A conventional three-electrode system was used with a glassy carbon working electrode, an Ag/AgCl (saturated KCl) reference electrode and a Pt wire counter electrode. Glassy carbon electrode (GCE) ( $d = 2.0$  mm and  $0.0314$  cm<sup>2</sup> geometric surface area) were purchased from Azar electrode Co. (Urmia, Iran). Electrochemical impedance spectroscopy (EIS) data were obtained by an Autolab PGSTAT 204 with an FRA software version 4.9 (Eco Chemie, the Netherlands). EIS measurements were conducted by applying an AC voltage with an amplitude of 10 mV and the frequency of 0.01 Hz to 20 kHz at OCP (open circuit potential). All experiments were performed at the room temperature.

Field emission scanning electron microscope (FESEM, model VEGA-Tescan, Razi Metallurgical Research Center, Tehran, Iran) equipped with an energy dispersive spectrometer (EDS) were used to evaluate the surface morphology and elemental composition of the prepared deposits. The transmission electron microscope (TEM) images were obtained using a PHILIPS CM 200 instrument. The FT-IR spectra of samples were recorded by using an ABB Bomem MB-100 FT-IR spectrophotometer using KBr pellets. Raman spectra were collected using Raman spectrometer (Senterra-Bruker) with a 785 nm laser excitation. An X-ray diffractometer (GBC MMA) using Cu K $\alpha$  irradiation was used for the preparation of X-ray diffraction (XRD) spectra. Inductively coupled plasma-optical emission spectroscopy data were acquired by ICP-OES, Vista-Pro, Varian Australia analyzer, after the dissolution of the sample in aqua regia. X-ray photoelectron microscopy (XPS) measurements were made on (X-Ray 8025, Bestec, Germany) with Mg K $\alpha$  radiation ( $h\nu = 1253.6$  eV).

Nitrogen adsorption/desorption measurements were carried out at 77 K at using micrometrics model ASAP2010 sorptometer to determine the surface area. Prior to N<sub>2</sub> adsorption, the samples were evacuated at 473 K under the vacuum condition. Specific surface areas were calculated from nitrogen adsorption data by multipoint Brunauer-Emmett-Teller (BET) theory. TGA (Thermo-gravimetric analysis) was used to determine the thermal stability of the synthesized materials and was carried out from room temperature to 873 K by using a TGA (Mettler Toledo 851) analyzer at a heating rate of 10 K/min under N<sub>2</sub> atmosphere.

## 2.3. Preparation of bimetallic Ni-Co/MOF, Ni/MOF, Co/MOF

Bimetallic Ni-Co/MOF was synthesized according to the reported work [31]. In a typical synthesis, 0.39 g Co(NO<sub>3</sub>)<sub>2</sub>·6H<sub>2</sub>O, 0.52 g NiCl<sub>2</sub>, and 0.168 g H<sub>2</sub>BDC were dissolved in 25.6 mL of DMF. The suspension was mixed thoroughly with magnetic stirring and ultrasonicated for 15 min at the room temperature until a homogeneous solution is

obtained. The resultant solution was transferred into a 100 mL Teflon-lined stainless steel autoclave, then capped tightly and placed in an oven at 135 °C for 15 h. After that, the autoclave was removed from the oven and allowed to cool down to room temperature. Finally, the resulting solid product was filtered and washed several times with DMF and ethanol. The product was dried in a vacuum oven overnight at 60 °C. A similar procedure, as described above, was applied for the preparation of Ni-MOF and Co-MOF, except that a single metal precursor was used.

## 2.4. Fabrication of NiCo/NiO-CoO/NPCC, Ni/NiO/NPCC, Co/CoO/NPCC modified electrodes

In the next step, the resulted bimetallic Ni-Co/MOFs was transferred into a ceramic boat and placed into a quartz tube, which was fixed in a furnace for thermal treatment. At first, the nitrogen flow was transferred continuously for 30 min over the sample to allow complete evacuation of air. Then furnace temperature was raised to 900 °C with a heating rate of 1 °C min<sup>-1</sup> for 8 h under the nitrogen atmosphere to obtain a black powder. The carbonized products were collected after cooling down to room temperature. The prepared nanocomposite in this step is notified as NiCo/NiO-CoO/NPCC. The preparation procedure is illustrated in Scheme 1. As the reference, Ni/NiO/NPCC, Co/CoO/NPCC were obtained with similar procedures from monometallic Ni/MOFs and Co/MOFs, respectively. For the electrode modification, the GCE surface was polished gently on a felt pad with alumina/water slurry to a mirror finish and later ultrasonically cleaned in ethanol for a few minutes to remove the residual alumina. Then, the electrode was rinsed thoroughly with distilled water. After that, 1.0 mg/mL homogeneous suspension was prepared by dispersing of 5.0 mg of the as-prepared catalyst in 5.0 mL ethanol with ultrasonic agitation. By using a microliter syringe, a 5  $\mu$ L portion of this mixture (without adding any binder and conductive agents) was directly casted onto the polished GCE and dried at the room temperature. The prepared electrode in this step is notified as NiCo/NiO-CoO/NPCC/GCE, Ni/NiO/NPCC/GCE, Co/CoO/NPCC/GCE. In the following for comparison, we also prepared Ni-MOF/GCE, Co-MOF/GCE, Ni-Co/MOF/GCE by a similar method as stated above (2  $\mu$ L nafion used as binder).

## 3. Results and discussion

### 3.1. Characterization of the synthesized materials

XRD analysis is used to identify the crystal phase and structural information of freshly prepared Ni/MOF, Co/MOF, Ni-Co/MOF and corresponding derivatives, after the carbonization, Ni/NiO/NPCC, Co/CoO/NPCC and NiCo/NiO-CoO/NPCC (Fig. 1A and B). As depicted in Fig. 1A, XRD results for Ni/MOF and Co/MOF are in agreement with those simulated from the single-crystal data of the sheet-like structures [Ni<sub>3</sub>(OH)<sub>2</sub>(C<sub>8</sub>H<sub>4</sub>O<sub>4</sub>)<sub>2</sub>(H<sub>2</sub>O)<sub>4</sub>]·2H<sub>2</sub>O (CCDC no. 638866) and MOF-71,

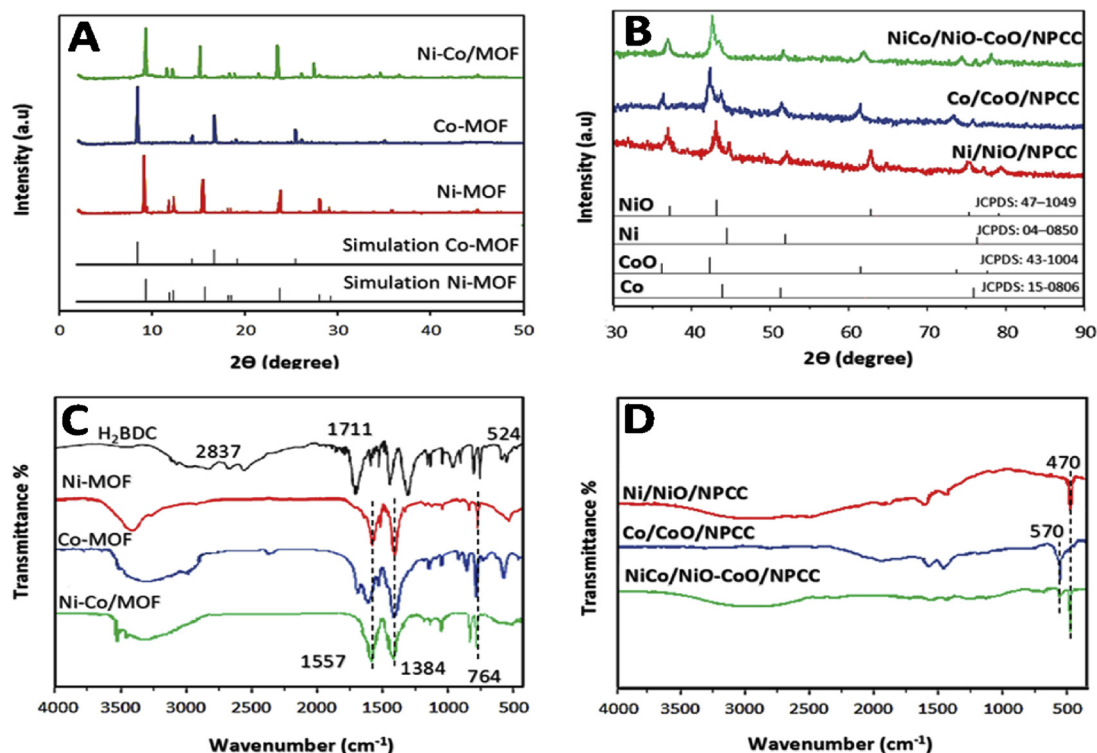


**Fig. 1.** Characterization results of the as-prepared samples: XRD patterns (A, B) and FTIR spectrum (C, D). Ni/MOF, Co/MOF Ni-Co/MOF (A, C) and Ni/NiO/NPCC, Co/CoO/NPCC, NiCo/NiO-CoO/NPCC (B, D).

same as previous reports, respectively [32,33]. Also, XRD patterns of as-synthesized Ni-Co/MOF matched exactly with Ni/MOF, suggesting that these MOFs have same layered topology in their crystal structures. Therefore, according to this result, it can be concluded that the crystalline structure of Ni-MOF could be retained after partial substitution by Co<sup>2+</sup> ions. In addition, Fig. 1B depicts XRD patterns of the obtained composites after the direct carbonization. In the pattern of Ni/NiO/NPCC, diffraction peaks at 42.8°, 49.2°, 63.14°, 72.57° and 88.11° can be indexed to (111), (200), (220), (311), and (222) planes of cubic phase of NiO (JCPDS card no. 47-1049), respectively [34]. Also, moreover to NiO peaks, three weak diffraction peaks at 44.4°, 1.3°, and 75.9°, corresponding to (111), (200), and (220) planes of face-centered cubic (fcc) phase of the crystalline Ni (JCPDS card no. 04-0850) are observed [35]. Moreover, in the pattern of Co/CoO/NPCC, well-defined diffraction peaks at 36.41°, 42.48°, 62.60° and 73.66° are ascribed to (111), (200), (220), and (311) planes of CoO (JCPDS card No. 43-1004). Also, three weak diffraction peaks can be observed at 44.37°, 51.47° and 75.66° corresponding to (111), (200) and (220) planes of Co (JCPDS card No. 15-0806) [36]. It is worth noting that in the case of NiCo/NiO-CoO/NPCC, due to the similar XRD patterns, all of the diffraction peaks with broader shape emerged between pure Ni, Co, NiO and CoO crystalline structure confirming mixing of metals (Ni-Co) and metal oxides (NiO-CoO) species in the resulted nanocomposite.

FT-IR spectra of the as-prepared MOFs powder and corresponding composites after thermal treatment are shown in Figs. 1C and D. Also, for comparison, the corresponding FT-IR spectrum for 1,4-H<sub>2</sub>BDC is shown in Fig. 1C. In the cases of Ni/MOF, Co/MOF and Ni-Co/MOF, the absorption peaks of the non-ionized carboxyl group of the free ligand 1,4-BDC, centered at 2837, 1711 and 524 cm<sup>-1</sup> corresponding to (OH), (C=O) and (C=O) groups, are not detected. Instead, two new absorption bands are appeared at around 1557 and 1384 cm<sup>-1</sup>, which describe asymmetric and symmetric stretching vibrations of carboxylate groups, respectively [31]. These results prove the complete deprotonation of acidic COOH upon reaction with metal ions. Meanwhile, the stretching vibration bands around 3250–3500 cm<sup>-1</sup> belong to H<sub>2</sub>O

molecules, proving the existence of coordinated H<sub>2</sub>O molecules in the as-prepared MOF. Moreover, a new peak is appeared at about 764 cm<sup>-1</sup>, which is related to the ring-out of-plane vibration of the 1,4-substituted benzene core of the linkers [37]. Clearly, the appearance of this peak exhibits a successful coordination between metal ions and BDC<sup>2-</sup> ligands. Also, it should be noted that a similar FT-IR pattern is observed for Ni-MOF and Ni-Co/MOF, which indicates that these MOFs are iso-structure and have a same layered topology. Furthermore, Fig. 1D shows FT-IR spectra of the composites obtained after the thermal treatment. Obviously, after the direct carbonization, the intensities of the MOFs peaks are considerably decreased, indicating that these groups have been decomposed after the thermal treatment. Also, two new peaks are appeared at 470 and 570 cm<sup>-1</sup>, which are corresponding to Ni–O and Co–O stretching vibrations in Ni/NiO/NPCC and Co/CoO/NPCC, respectively. Moreover, NiCo/NiO-CoO/NPCC clearly shows these new peaks, which confirmed the presence of both two metal oxides in the obtained composite.

In order to investigate the surface morphology, the obtained FESEM images are shown in Fig. 2. According to the FESEM image (Fig. 2A), it can be clearly seen that petal-like Ni-Co/MOF nanosheets were gathered together to form flowerlike structures. This ultimate porous 3D flowerlike structure is consisting of cross-linked porous sheet-like sub-units, which have relatively a smooth surface and estimated thickness for them are about 30 nm. These thin sheets are reconnected in different orientations with obvious open spaces between adjacent nanosheets. Moreover, Fig. 2B shows the FESEM image of NiCo/NiO-CoO/NPCC, which almost exhibits a similar morphology as Ni-Co/MOF precursor. It can be concluded that the carbonization process does not induce a remarkable impact in the appearance of NiCo/NiO-CoO/NPCC except that thickness of nanosheets decreases and reaches to about 10 nm. Importantly, it was speculated that these 3D unique structures optimize the electrochemical performance of the electrode materials, because provide the effective electrode/electrolyte contact throughout the whole electrode structure and creates more active sites available for the electro-oxidation reaction. Also, elemental mapping presented next to

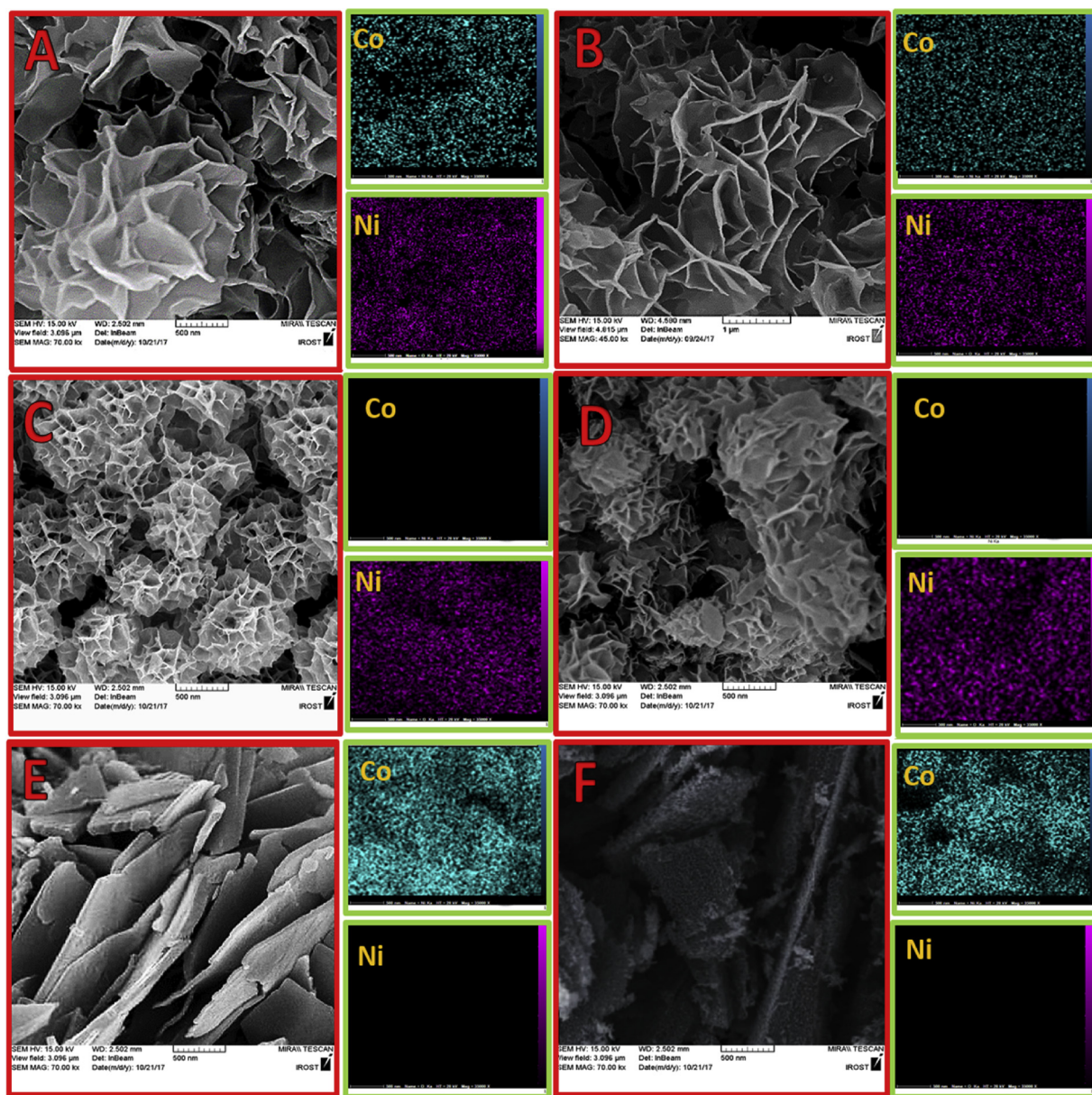


Fig. 2. SEM images and elemental mapping of (A) Ni-Co/MOF, (B) NiCo/NiO-CoO/NPCC, (C) Ni/MOF, (D) Ni/NiO/NPCC, (E) Co/MOF, (F) Co/CoO/NPCC.

the FESEM image reveals the presence and uniform distribution of Ni and Co elements throughout the entire prepared MOFs and related carbonized composites. In the following, for comparison, Figs. 2C and D displays the FESEM images for Ni-MOF and Ni/NiO/NPCC, respectively. It can be observed that Ni-MOF with a flower shape composed of porous spherical-type structures with interconnected thin nanosheets. Also, Fig. 2D indicates that after the direct carbonization, the original flower-like morphology of Ni-MOF was perfectly kept. The elemental mapping confirmed the uniform distribution of Ni without another impurity. In addition, the FESEM of Co-MOF and Co/CoO/NPCC are shown in Fig. 2E and F. The image shows that Co-MOF was composed of 2D thin nanosheets with about 150 nm thicknesses and a homogeneous laminar structure. It can be seen that Co/CoO/NPCC basically maintained the original shape after the direct carbonization, but the nanosheet surface become coarse with Co/CoO nanoparticles. Also, elemental mapping results clearly showed that Co was homogeneously distributed in the prepared samples.

Also, to further investigate the nanoscale morphology of Ni-Co/MOF and NiCo/NiO-CoO/NPCC, TEM analysis was adopted (Fig. 3).

According to Fig. 3A and B, it can be seen that Ni-Co/MOF consisted of many randomly thin nanosheets in different directions. These nanosheets with transparent features indicate the ultrathin nature of the petal-like structure. Due to the much larger lateral size of the nanosheets than its thickness, the morphologies of bending, curling, and crumpling are clearly observed. The visible dark strips are generally folded edges, wrinkles or ripples of the nanosheets. Also, for studying the effect of the carbonization process on the structure of the obtained MOFs, TEM images of NiCo/NiO-CoO/NPCC presented in Fig. 3C and D. It can be seen that, the basic sheet-like structure of precursors is maintained after thermal treatment. Also, a closer look in Fig. D, shows uniform dispersion of metal (Ni, Co) and metal oxide (NiO, CoO) nanoparticles, which embedded in the carbon matrix after the carbonization process. Moreover, the inset in Fig. 3D precisely shows numerous nearly uniform nanoparticles on the edge of nanosheets.

In order to explore further evidences for the elemental composition and the oxidation states of the as-synthesized NiCo/NiO-CoO/NPCC, the XPS measurements were performed (Fig. 4). The survey scan spectrum indicates the presence of Ni, Co, and O as well as carbon and

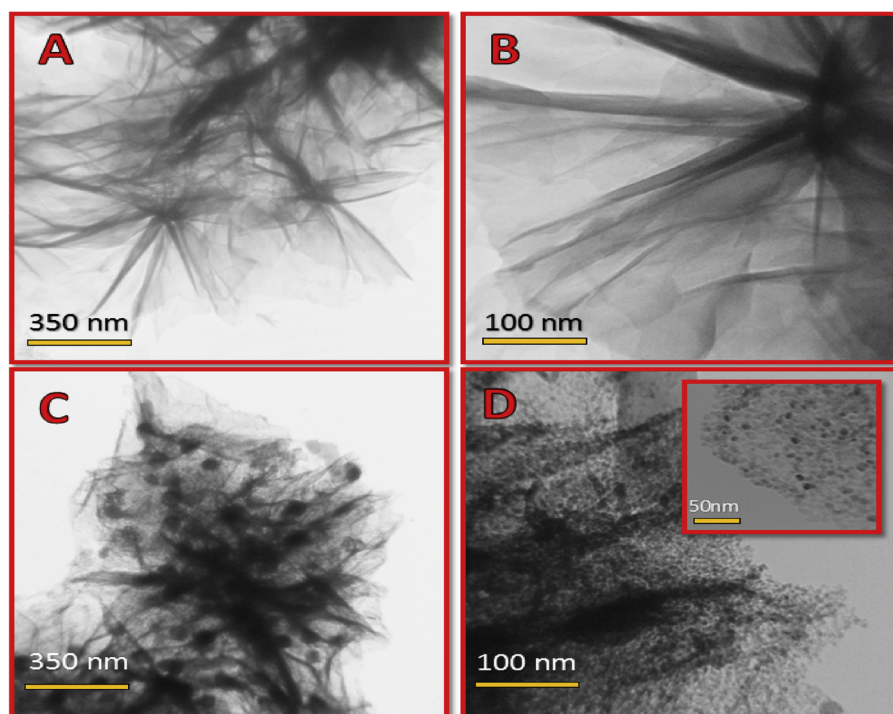


Fig. 3. TEM images of the Ni-Co/MOF NPC (A, B) and NiCo/NiO-CoO/ (C, D).

the absence of other impurities (Fig. 4A). According to the XPS analysis, in the case of Ni, two typical peaks are located at 854.2 and 872.1 eV, which can be assigned to the spin-orbit splitting of  $2p_{3/2}$  and  $2p_{1/2}$ , respectively (Fig. 4B). Moreover, two other peaks centered at around 859.8 and 878.8 eV belong to Ni  $2p_{3/2}$  and  $2p_{1/2}$  shakeup satellites, respectively. As shown in Fig. 4B, four fitting peaks located at binding energies of 853.4, 855.7 and 871.6 and 873.3 eV were observed in the

deconvoluted XPS spectrum of Ni  $2p$ , which are related to Ni(0) and Ni (II) [38]. Also, the detailed spectrum of the Co  $2p$  peaks is presented in Fig. 4C. This spectrum is typically separated into  $2p_{3/2}$  (780.26 eV) and  $2p_{1/2}$  (797.3 eV), due to the spin-orbit coupling energy states and accompanied by two satellite peaks (785.7 and 802.3 eV). In the deconvoluted XPS spectrum of Co  $2p$ , four peaks with binding energies values of 777.6, 780.4, 795.3, and 797.6 eV could be clearly specified that are

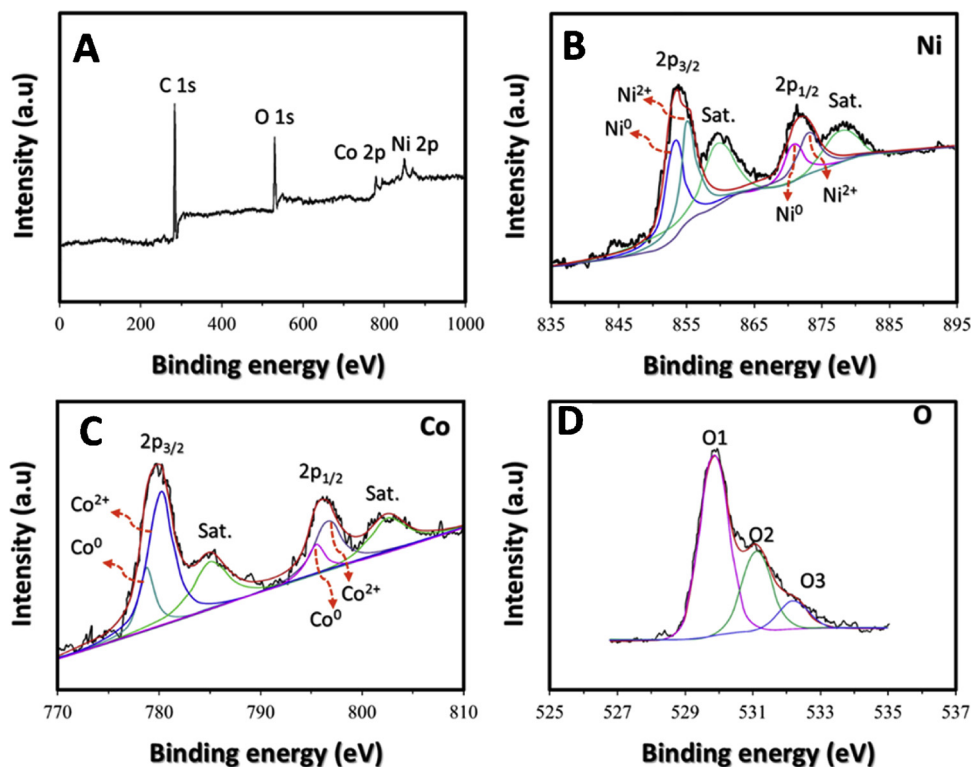


Fig. 4. XPS survey (A) and high-resolution XPS spectra of Ni 2p (B), Co 2p (C), O 1s (D), for the NiCo/NiO-CoO/NPCC.

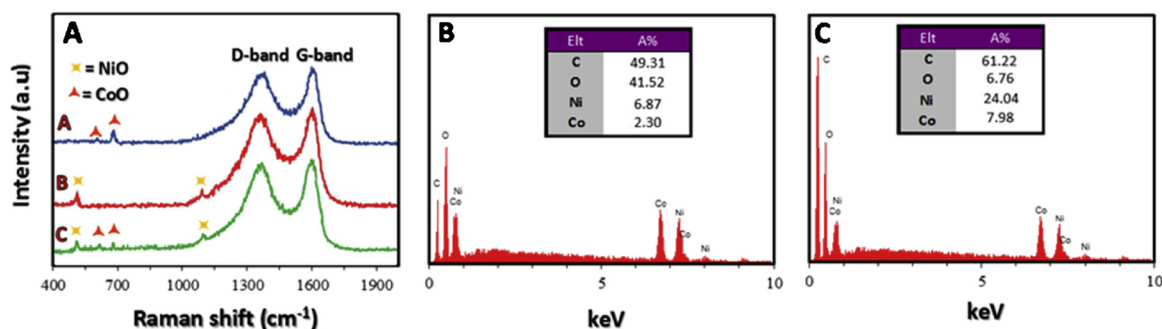


Fig. 5. (A) Raman spectra of (A) Co/CoO/NPCC, (B) Ni/NiO/NPCC, and (C) NiCo/NiO-CoO/NPCC. Energy dispersive spectra: Ni-Co/MOF (B) and NiCo/NiO-CoO/NPCC (C).

belong to Co(0) and Co (II) [39]. Moreover, in the deconvoluted XPS core level spectrum of O 1s, three oxygen bonding features (O1, O2, and O3) could be evidently distinguished (Fig. 4D). The O1 peak at 529.7 eV could be assigned to lattice oxygen and is corresponding to the metal oxygen bond in NiO and CoO. The peak at 531.5 eV (O2) corresponds to defective sites and oxygen deficient regions in the metal oxide preparations. Furthermore, O3 at 532.7 eV can be ascribed to physico/chemically adsorbed water on the surface of the samples [40].

For a more precise investigation, the Raman spectra of Ni/NiO/NPCC, Co/CoO/NPCC and NiCo/NiO-CoO/NPCC have exhibited in Fig. 5A. In all cases, two prominent peaks at around 1352 cm<sup>-1</sup> and 1600 cm<sup>-1</sup> are observed that assigned to the vibration modes of D and G bands, respectively. The intensity ratio of D and G bands ( $I_D/I_G$ ) shows the degree of graphitization of carbon materials [36]. The obtained values for  $I_D/I_G$  in all spectra are implying a similar degree of the graphitization. Moreover, in the spectrum of Co/CoO/NPCC two new peaks at 594 and 681 cm<sup>-1</sup>, related to the Co-O stretching vibration of CoO are appeared [41]. In addition, Ni/NiO/NPCC shows two characteristic stretching vibrations of Ni – O around 532 and 1090 cm<sup>-1</sup> [42]. Meanwhile, it is found that NiCo/NiO-CoO/NPCC shows the Ni – O and Co-O stretching vibration peaks in the spectrum, which indicates that the obtained composite is containing mixed metal oxides. Furthermore, EDS analysis was further conducted to examine the element composition of Ni-Co/MOF and NiCo/NiO-CoO/NPCC. It can be seen from Fig. 5 (B and C) that C, O, Co and Ni elements co-exist in the samples, revealing that Co has been successfully incorporated in the structure of Ni-MOF. Also, quantitative analysis by EDS confirmed that the mole ratio of Ni/Co was about 2.98 and 3.01 in Ni-Co/MOF and NiCo/NiO-CoO/NPCC, respectively. Moreover, ICP analyses were carried out for precise measuring the Ni/Co mole ratio. The obtained elemental analysis was 2.98 and 3.08 for Ni-Co/MOF and NiCo/NiO-CoO/NPCC, respectively, which was in agreement with the obtained results from EDS analysis.

In the following, BET measurements were conducted to evaluate the specific surface areas and porosity of the MOFs and the related carbonized composites. Adsorption/desorption isotherms and corresponding pore size distribution plots of the synthesized compounds are shown in Fig. 6A to C and the obtained data are summarized in Table 1. As can be seen in traces (A–C), according to the International Union of Pure and Applied Chemistry (IUPAC) classification, the isotherms depicted typical IV type curves with H4 type hysteresis behavior, which represent a mesoporous structure [43]. It also found that among the obtained MOFs and the carbonized products, Ni-Co/MOF and NiCo/NiO-CoO/MOF show higher BET specific surface areas. In addition, due to the aggregation of numerous nanoparticles to form a porous structure, the carbonization process generated abundant mesoporosity, leading to the higher surface area. Moreover, the pore size distribution of Ni-Co/MOFs samples is narrow with a single modal 1.7 nm. After the direct carbonization, because of the removing the ligands and expansion of the pores, the pores size became larger and broader and reaches to 19 nm

[44]. It is worth to mention that, due to more active sites within the pores, the large surface area and mesoporous structure are favorable characteristics for fast electrochemical reactions. Such outstanding properties allow efficient contact between catalysts and electrolyte, and as a result, fast transfer of electrons/ions, which finally enhances the overall electrochemical performance.

Furthermore, thermal stability of the synthesized MOFs was investigated by the TGA curve at N<sub>2</sub> atmosphere (Figs. 6D to F). As can be seen in Fig. 6, all of the MOFs samples displayed a similar TGA curve. The weight loss was observed at two main steps: the first weight loss in the temperature range of 100 to 200 °C arose from evaporation of moisture and embedded solvent. The second weight loss between 300 to 350 °C resulted from the decomposition of the organic linkers. After 400 °C, the curves have no obvious weight loss process. Therefore, the framework began to decompose from 350 °C, and then remnant materials completely carbonized at higher temperatures and finally metal/metal oxides nanoparticles distributed in carbon frame yielded under N<sub>2</sub> atmosphere [27].

### 3.2. Electrochemical properties of the prepared MOFs and related carbonized composites

Cyclic voltammetry was used to characterize the electrochemical behavior of the prepared modified electrodes. Fig. 7A depicts the cyclic voltammograms (CVs) of Ni/MOF/GCE, Co/MOF/GCE and Ni-Co/MOF/GCE recorded in 0.5 M NaOH solution at a scan rate of 50 mVs<sup>-1</sup>. As can be seen in this figure, the CVs profile of the Ni/MOF exhibits well-defined anodic and cathodic peaks associated with Ni<sup>2+</sup>/Ni<sup>3+</sup> redox couple [45]. In the case of Ni-Co/MOF/GCE, the voltammetric behavior of the bimetallic MOF is mainly similar to that of Ni/MOF/GCE, except that CV profile shows a lower onset potential and higher current density. The results implied that the presence of Co<sup>2+</sup> in the structure of the Ni/MOF/GCE has been significantly improved the electrochemical performance of the bimetallic MOF. Moreover, the Co/MOF/GCE exhibited two pair of redox peaks relating to transitions of Co<sup>2+</sup>/Co<sup>3+</sup> and Co<sup>3+</sup>/Co<sup>4+</sup>, respectively (inset of Fig. 7A) [46]. Also, for more information and precise comparison, CVs measurements were performed for Ni/NiO/NPCC/GCE, Co/CoO/NPCC/GCE, and NiCo/NiO-CoO/NPCC/GCE and the obtained results are presented in Fig. 7B. It is obvious that, in contrast to their related MOFs, the carbonized composites show significantly higher current densities. The resulted improvement in the electrochemical performance can be related to the synergistic effect of metal/metal oxides and carbon framework. Also, according to the obtained CV profiles, the possible reactions mechanism could be interpreted by the following explanation:

In the case of Ni/NiO/NPCC/GCE, a pair of well-defined redox peaks ( $a_1$  and  $a_2$ ) can be described according to the following reactions [29]:



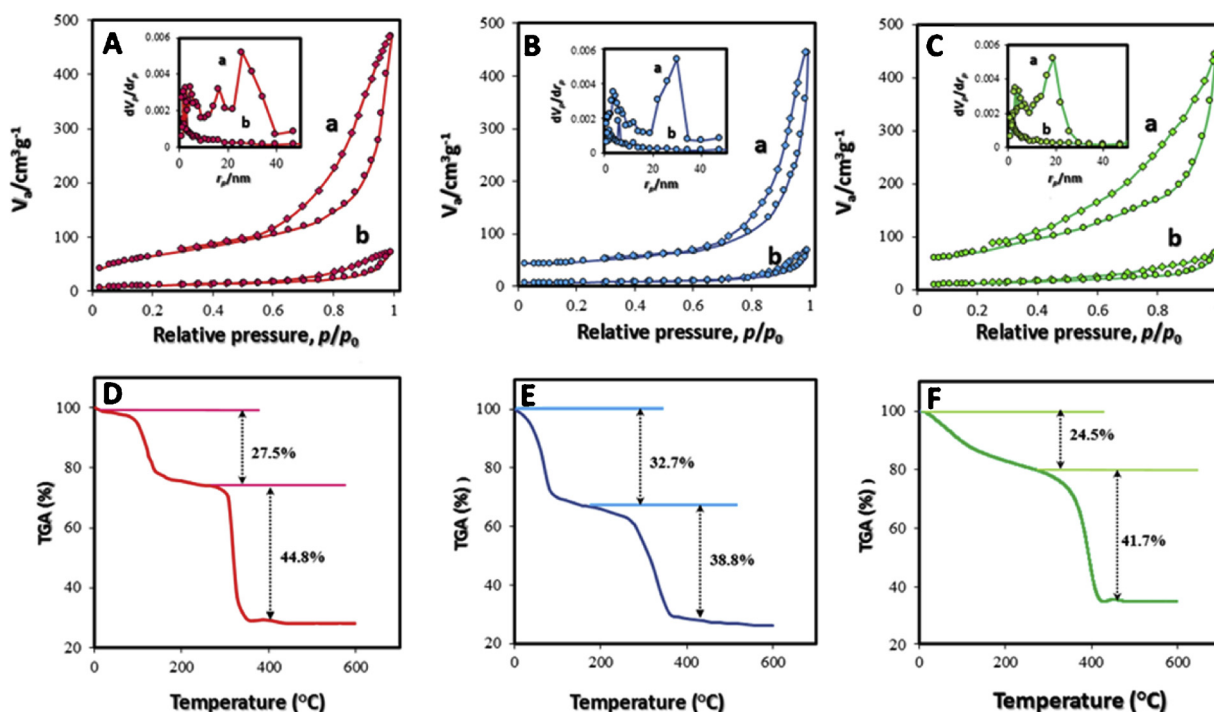
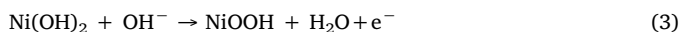


Fig. 6. N<sub>2</sub> adsorption and desorption isotherms of (A): Ni/NiO/NPCC (a) and Ni/MOF (b), (B): Co/CoO/NPCC (a) and Co/MOF (b), (C): Ni-Co/MOF (a) and NiCo/NiO-CoO/NPCC (b). Inset: the pore size distributions of the samples. TGA and DTG curves of the Ni/MOF (D), Co/MOF (E), Ni-Co/MOF (F).

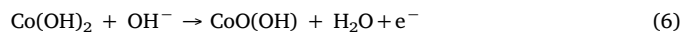
Table 1

BET surface areas, pore volumes, and pore sizes for the synthesized samples.

Sample	BET surface area (m <sup>2</sup> g <sup>-1</sup> )	Total pore volume (cm <sup>3</sup> g <sup>-1</sup> )	Pore size (nm)
Ni/MOF	289	0.321	1.7
Co/MOF	117	0.297	1.67
Ni-Co/MOF	414	0.493	1.61
Ni/NiO/NPCC	390	0.452	25.3
Co/CoO/NPCC	273	0.340	29.2
NiCo/NiO-CoO/NPCC	543	0.580	19.2



Apparently, for Co/CoO/NPCC/GCE/GCE two pair of redox peaks (p<sub>1</sub>, p<sub>2</sub>) can be observed based on the reversible transitions of Co<sup>2+</sup>/Co<sup>3+</sup> and Co<sup>3+</sup>/Co<sup>4+</sup> redox couples as follows [38]:



Noticeably, NiCo/NiO-CoO/NPCC/GCE exhibited three pairs of redox peaks. The redox couples b<sub>1</sub>/b<sub>4</sub>, b<sub>2</sub>/b<sub>5</sub> and b<sub>3</sub>/b<sub>6</sub> are associated to the Co<sup>2+</sup>/Co<sup>3+</sup>, Co<sup>3+</sup>/Co<sup>4+</sup>, and Ni<sup>2+</sup>/Ni<sup>3+</sup> reactions, respectively. The possible reaction mechanism could be represented by the following reaction:

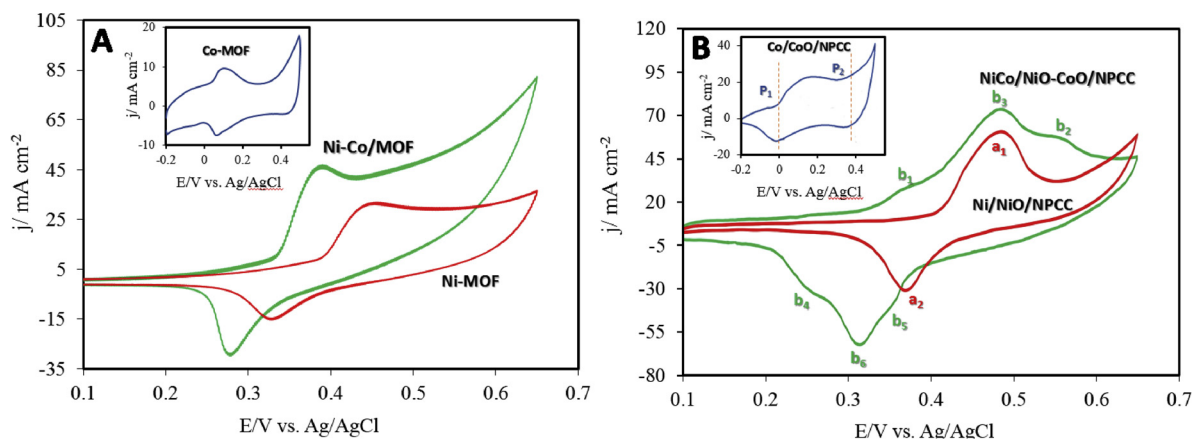


Fig. 7. The CV curves of (A) Ni/MOF/GCE and Ni-Co/MOF/GCE, (B) Ni/NiO/NPCC/GCE, NiCo/NiO-CoO/NPCC/GCE and Inset: (A) Co/MOF/GCE and (B) Co/CoO/NPCC/GCE in 0.5 M NaOH solution at ν = 50 mVs<sup>-1</sup>.

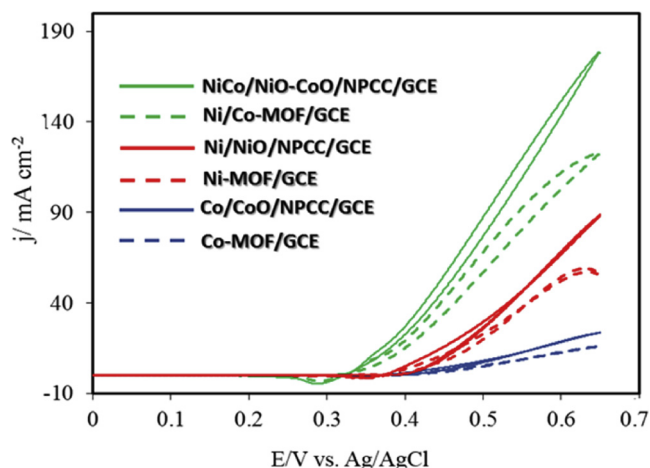
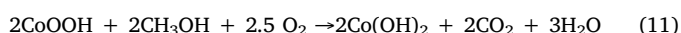
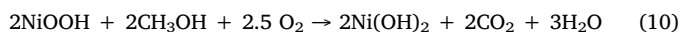


Fig. 8. Electrochemical responses of Ni-Co/MOF/GCE, Ni/MOF/GCE, Co/MOF/GCE, NiCo/NiO-CoO/NPCC/GCE, Ni/NiO/NPCC/GCE and Co/CoO/NPCC/GCE in 0.5 M methanol + 0.5 M NaOH solution at  $\nu = 50 \text{ mVs}^{-1}$ .

### 3.3. Electrocatalytic oxidation of methanol

In continuance, the electrocatalytic activities of the prepared MOFs and related carbonized composites towards the methanol oxidation reaction (MOR) were investigated. Fig. 8 presented the typical CVs curves recorded for the methanol electro-oxidation in a solution containing 0.5 M methanol and 0.5 M NaOH at a scan rate of  $50 \text{ mV s}^{-1}$ . In comparison to Fig. 7A and B, investigations in the absence of methanol, an increment in the anodic peak current density together with decreasing of the cathodic peak current during the reverse scan are the main effects observed upon methanol addition to the electrolyte solution. Therefore, the electrocatalytic performance of these electrodes for MOR was assessed by comparing their corresponding peak current densities ( $j_p$ ) towards the methanol oxidation. It can be seen that anodic peak current densities are increasing in the order of NiCo/NiO-CoO/NPCC/GCE > Ni/NiO/NPCC/GCE  $\approx$  Ni-Co/MOF/GCE > Ni/MOF/GCE > Co/CoO/NPCC/GCE > Co/MOF/GCE. According to this result, addition of a second metal in the MOF structure can lead to enhancement of the electrocatalytic activity of the bimetallic MOFs. In addition, it is obvious that after the carbonization process, collaboration between highly conductive porous carbon framework and mixed metal/metal oxides increases the catalytic efficiency of the obtained composite. Therefore, these cases should be taken into account as two main factors for the evaluation of the catalytic capability of the prepared modified electrode. The accepted mechanism for MOR on NiCo/NiO-CoO/NPCC/GCE may be simply illustrated by the following reactions, respectively [20]:



Furthermore, another point that can be deduced from the CVs profiles is that start potential ( $E_{\text{onset}}$ ) for the methanol electro-oxidation on the surface of NiCo/NiO-CoO/NPCC/GCE modified electrode is much lower than the other prepared modified electrodes. This behavior meaning that, NiCo/NiO-CoO/NPCC/GCE has much lower over-potential and effectively improves the kinetics of the methanol oxidation reaction. So, according to the mentioned results, the electrocatalytic performance of NiCo/NiO-CoO/NPCC/GCE is much better than those of other prepared catalysts. Also, for a more precise comparison, the electrocatalytic parameters ( $j_f$  and  $E_{\text{onset}}$ ) obtained from CVs of the modified electrodes were summarized in Table 2.

Regarding all of the experimental facts and the above presented analysis, reasonable explanations about the improved electrocatalytic performance of NiCo/NiO-CoO/NPCC/GCE can be classified as follows:

Table 2

Electrochemical characteristics of methanol oxidation on different prepared catalysts in solution containing 0.5 M NaOH and 0.5 M methanol at  $50 \text{ mV s}^{-1}$ .

Electrocatalyst	$E_{\text{onset}}$ (V)	$j_f$ ( $\text{mA cm}^{-2}$ )
Ni/MOF/GCE	0.41	55
Co/MOF/GCE	0.46	15
Ni-Co/MOF/GCE	0.34	122
Ni/NiO/NPCC/GCE	0.38	87
Co/CoO/NPCC/GCE	0.43	23
NiCo/NiO-CoO/NPCC/GCE	0.32	178

(1) There is a close correlation between the shape/morphology and the catalytic activity of the prepared electrocatalysts. So, unique petal-like nanostructures with enlarged specific surface area provide more accessible active sites for MOR, which leads to enhancement of the electrocatalytic activity. On the other hand, petal-like structures consist of interconnected nanosheets with porous architecture offer short diffusion paths for electrons/ions transport, which leads to a faster kinetics, lower overpotential and higher electro-catalytic activity.

(2) It is known that the composition of catalysts mainly determines their catalytic activities. Therefore, in the obtained composite, mixed Ni/Co metals and NiO/CoO metal oxides can provide a potential synergistic effect (including bifunctional and electronic effects), which leads to a higher electro-catalytic reactivity. The bifunctional effects endow the efficient adsorption of the  $\text{OH}_{\text{ad}}$  species and complete removal of the adsorbed carbon oxide ( $\text{CO}_{\text{ad}}$ ) to improve the catalyst stability. On the other hand, the electronic effects have some influences on the chemisorption energy of the adsorbed intermediates on the catalysts. Also, the electronic effects can facilitate the electron transport between the metals/metal oxides to increase the electrocatalytic performance.

(3) Also, appropriate support plays a prominent role on the electrochemical behavior of a catalyst, owing to the surface reactivity and support-catalyst interaction. In this regard, porous carbon framework obtained after the carbonization of MOFs facilitates electron transfer kinetics and enlarges the surface active area.

(4) Moreover, high loading and good dispersion of catalysts nanoparticles in the modifier film on the electrode surface has a notable impact on the electrocatalytic activity of the fabricated modified electrode. Hence, in situ preparation of mixed metals/metal oxides in carbon framework after MOFs carbonization process is a beneficial approach in formation of uniform nanoparticles embedded in the carbon template, which avoids the agglomeration or growing of metals/metal oxides into larger particles.

Also for a precise insight, the electrocatalytic activities of NiCo/NiO-CoO/NPCC/GCE in terms of the kinetic parameters are listed in Table 3, and the values are compared with some previous works.

### 3.4. Electrochemical impedance spectroscopic studies

The electrochemical impedance spectroscopy (EIS), as a valuable electrochemical technique, was used for studying the conductivity and ion transport/diffusion ability on the surface of the prepared electrodes. Fig. 9A and B illustrates the Nyquist diagrams for various electrodes including Ni/MOF/GCE, Co/MOF/GCE and Ni-Co/MOF/GCE and Ni/NiO/NPCC/GCE, Co/CoO/NPCC/GCE, NiCo/NiO-CoO/NPCC/GCE, respectively. The EIS was performed in the frequency range from 0.01 Hz to 100 kHz with ac amplitude of 10 mV and equilibrium time of 1 s in 0.1 M KCl electrolyte containing equimolar of  $\text{Fe(CN)}_6^{3-/4-}$  ions (5 mM). These Nyquist plots mainly consisted of a semicircle at the high-frequency region and followed by a straight line at the low-frequency region and a Warburg slope of  $45^\circ$  in the middle frequency region between the semicircle and the straight line.

The semicircle is related to the electron transfer limiting step and

**Table 3**

Comparison of the parameters for electrocatalytic oxidation of ethanol at NiCo/NiO-CoO/NPCC/GCE with several chemically modified electrodes.

Electrode	Modifier	$\nu$ (mVs <sup>-1</sup> )	$E_{\text{onset}}^a$ (V)	$E_p^a$ (V)	$j^b$ (mA cm <sup>-2</sup> )	Ref.
GCE	NiO/Ni-P	50	0.32	0.5	28.56	[47]
Carbon	NiO-HS	5	0.35	0.56	25.1	[48]
GCE	Ni(II)Co(II) salen	10	–	0.58	7.05	[49]
GCE	NiCo-P-O	50	0.31	0.6	39.90	[50]
Ti foil	Ni <sub>2</sub> Co <sub>2</sub>	50	–	0.65	58	[51]
Nickel Foam	Co <sub>3</sub> O <sub>4</sub> /NiO	25	0.2	–	143	[52]
GCE	MnO <sub>x</sub> /NiO <sub>x</sub>	20	0.32	0.6	8.21	[53]
Stainless steel	NiCo <sub>2</sub> O <sub>4</sub>	10	0.27	0.5	125	[54]
Stainless steel	NiCo <sub>2</sub> O <sub>4</sub>	10	0.29	0.5	98	[55]
GCE	NiCo/NiO-CoO/NPCC/GCE	50	0.28	0.61	178	This work

<sup>a</sup> Eonset and Ep vs. SCE.

<sup>b</sup> Current density:  $j$  = peak current/A (A is the geometric surface area of substrate).

diameter of the semicircle reflected charge-transfer resistance ( $R_{\text{ct}}$ ) [56]. As shown in the inset of Fig. 9A, the semicircle diameter for Ni-Co/MOF/GCE is smaller than Ni-MOF/GCE and Co-MOF/GCE, indicating the lower electron transfer resistance and considerably enhanced kinetics on the surface of the bimetallic MOFs. Also, the low frequency straight line should display vertical shape with slopes close to 90° for an ideal capacitor. The deviation is caused by the diffusive behavior of the electrolyte in the electrode pores [36]. It can be seen that, slope of the straight line for Co/Ni-MOF/GCE is higher than Ni-MOF/GCE and Co-MOF/GCE, indicating the faster kinetics of the diffusion process. The Warburg slope is associated with the limitations of ion diffusion/transport in the electrode surface. It is observed that Ni-Co/MOF/GCE shows the shortest Warburg length, which suggests the fast diffusion and quick adsorption of ions from the solution onto the electrode surface. It can be concluded that the petal-like structure of Ni-Co/MOF/GCE with high surface area and accessible active sites provides shorter diffusion paths and fastest ion transport kinetics [57]. Also, Fig. 9B shows the Nyquist plots for prepared composites after the carbonization process of all three MOFs samples. It can be observed that, there is an obvious difference between the impedance patterns of the obtained composites and related MOFs. Comparison between impedance profiles of composites and related MOFs indicates that Ni/NiO/NPCC/GCE, Co/CoO/NPCC/GCE and NiCo/NiO-CoO/NPCC/GCE shows smaller semicircle diameter and steeper straight line. This result suggests faster electron transfer and enhanced ion diffusion process after the carbonization process. Finally, the aforementioned results indicate that the electron conductivity and ions transport of NiCo/NiO-CoO/NPCC/GCE is much better than the other prepared catalysts. This

result can be attributed to the presence of NiCo and NiO-CoO nanoparticles in the petal-like structure with a higher surface area. Also, the presence of carbon framework, as a high electrical conductive material, facilitates the electron transfer process [36].

### 3.5. Long-term stability

From practical view, besides the required high electrocatalytic activity for a catalyst, long-term stability of the fabricated modified electrode is also important for their real applications in DMFCs. Hence, in order to compare the long-term activity and durability of the prepared MOFs and related carbonized composites, chronoamperometry measurements were conducted in a solution containing 0.5 M methanol and 0.5 M NaOH for 2000s at the peak potential value corresponding to the forward peaks in the CVs (Fig. 10A). It can be seen that the current densities for all samples drop quickly at the initial stage of the experiment. However, when the time is above 200 s, the current density reaches to a relatively stable value. As observed, the carbonized composite catalysts show higher activities and durability as compared to their related MOFs. It is obvious that, in comparison with the other prepared catalysts, NiCo/NiO-CoO/NPCC/GCE exhibits lowest rate of current decay and higher current densities over the entire time period. Therefore, it can be concluded that, the electrode modified with NiCo/NiO-CoO/NPCC/GCE has the best electrocatalytic stability and poisoning tolerance against the methanol electro-oxidation in alkaline medium. The above results are consistent with the CV data shown in Fig. 8. Moreover, the stability of NiCo/NiO-CoO/NPCC/GCE catalyst was further evaluated by observing the variation of anodic peak current densities with the number of potential scan cycles. In this way, a total of 300 potential scans between 0 and 0.65 V were done in the solution containing 0.5 M methanol and 0.5 M NaOH and the evolution of the peak current density was monitored (Fig. 10B). As shown in this figure, the CV curve is quite stable after 300 cycles and the anodic current density is about 93% than that 5<sup>th</sup> scan, demonstrating its excellent cycle stability. Also, for more information, features of NiCo/NiO-CoO/NPCC/GCE surface were observed by SEM after 300 consecutive cycles (Fig. 10B inset). According to the obtained results, some defect and crumpling on the edge of nanosheets could be clearly observed. However, the nanocomposite has retained its original petal-like nanosheets structure.

### 3.6. Effects of methanol concentration and potential sweep rates

In order to evaluate the capacity of NiCo/NiO-CoO/NPCC/GCE for methanol oxidation, the effect of methanol concentration on the corresponding peak currents in 0.5 M NaOH solution was investigated (Fig. 11A). It is generally recognized that the magnitude of peak current density is directly proportional to the amount of methanol that oxidized at the electrode surface. Plot of the peak current densities versus the

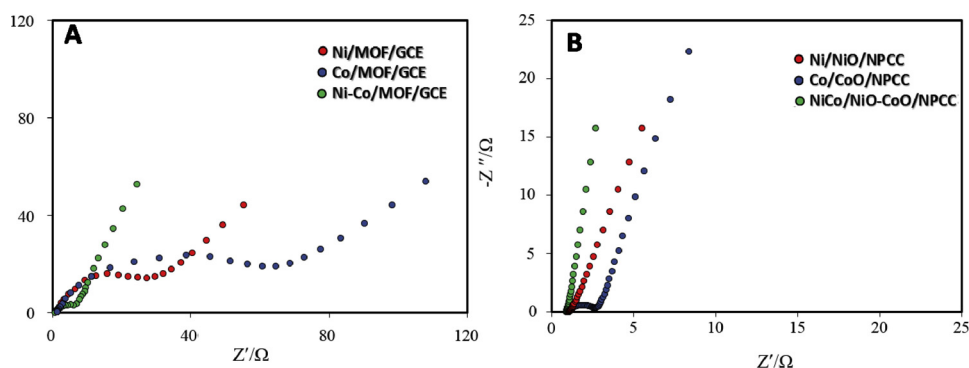


**Fig. 9.** Nyquist plots of impedance measurements in 5.0 mM  $K_3[Fe(CN)_6]/K_4[Fe(CN)_6] + 0.1$  M KCl solution performed on the (A) Ni-Co/MOF/GCE, Ni-MOF/GCE, Co-MOF/GCE and (B) NiCo/NiO-CoO/NPCC/GCE, Ni/NiO/NPCC/GCE and Co/CoO/NPCC/GCE.

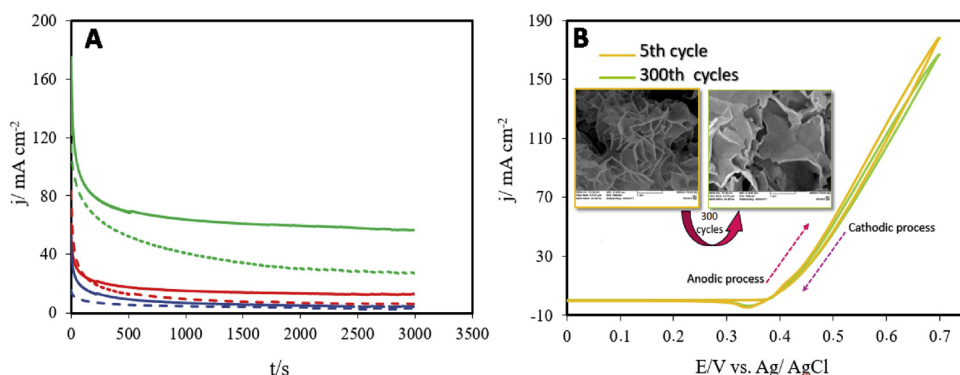


**Fig. 10.** (A) Chronoamperograms of the Ni-Co/MOF/GCE, Ni/MOF/GCE, Co/MOF/GCE, NiCo/NiO-CoO/NPCC/GCE, Ni/NiO/NPCC/GCE and Co/CoO/NPCC/GCE in 0.5 M NaOH + 0.5 M ethanol solution at peak potential values. (B) CVs of NiCo/NiO-CoO/NPCC/GCE from 5<sup>th</sup> to 300<sup>th</sup> cycle in 0.5 M NaOH + 0.5 M ethanol solution at  $\nu = 50 \text{ mVs}^{-1}$  (inset: SEM image for NiCo/NiO-CoO/NPCC/GCE after 300 cycles).

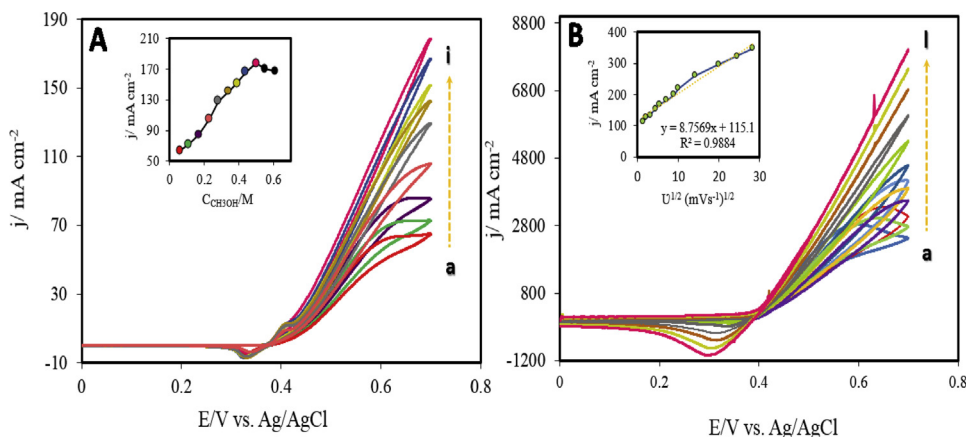


**Fig. 11.** (A) CVs of NiCo/NiO-CoO/NPCC/GCE for the electro-oxidation of methanol in different concentration (0.06–0.61 M) in 0.5 M NaOH solution at  $\nu = 50 \text{ mVs}^{-1}$ . Inset: Plot of forward anodic peak current density vs. methanol concentration (0.06–0.61 M). (B) CVs of NiCo/NiO-CoO/NPCC/GCE for the electro-oxidation of methanol at different scan rates (2–800  $\text{mVs}^{-1}$ ) in 0.5 M NaOH + 0.5 M ethanol solution. Inset: Plot of forward anodic peak current density vs. square root of scan rate.

methanol concentration shows a linear increase in the range of 0.06–0.50 M and decreases at concentrations higher than 0.5 M (inset 10 A). In accordance with this result, the optimum methanol concentration to achieve a higher peak current density might be considered as about 0.5 M. Also, the effect of potential scan rates is studied on the electrocatalytic oxidation of methanol at the surface of NiCo/NiO-CoO/NPCC/GCE. Fig. 11B shows recorded CVs at different scan rates (2–1000  $\text{mVs}^{-1}$ ) in 0.5 M methanol and 0.5 M NaOH solution. It can be seen that a linear relationship is obtained when peak current density values are plotted against the square root of the potential scan rate ( $\nu^{1/2}$ ) (inset of Fig. 11B). This behavior displays that the electro-oxidation of methanol is a diffusion controlled process [58].

#### 4. Conclusions

The main purpose of this study is to present a new strategy for preparation of a novel nonprecious catalyst containing mixed transition metals/metal oxides in nanoporous carbon frame by using mixed MOFs as a precursor's material. In summary, Ni-Co/MOF/GCE were prepared through a facile hydrothermal approach and NiCo/NiO-CoO/NPCC/GCE were fabricated after carbonization process of bimetallic MOFs. In the following, for comparison, Ni-MOF/GCE and Co-MOF/GCE and related composites Ni/NiO/NPCC/GCE and Co/CoO/NPCC/GCE were prepared by a similar method. The obtained results approved that after the carbonization process, the MOFs template and organic constituents were completely decomposed. The XRD pattern of the carbonized composites sample showed that metallic nanoparticles in MOF precursors converted to mixed transition metals/metal oxides nanoparticles, which uniformly embedded in the carbon frame. The FE-SEM results showed that NiCo/NiO-CoO/NPCC/GCE has a unique petal-like structure consisting cross-linked porous sheet-like subunits. However, the structures of Ni/NiO/NPCC/GCE and Co/CoO/NPCC/GCE were completely different and show flower shape and 2D thin nanosheets

structure, respectively. The result of EIS revealed that, by introducing second metal to the Ni-MOF structure and carbonization process and producing the multi-component composite containing NiCo/NiO-CoO and carbon template, the Rct for the electrode process is decreased. The electroactivity of NiCo/NiO-CoO/NPCC/GCE studied towards methanol oxidation using various electrochemical techniques and compared with properties of Ni/NiO/NPCC/GCE and Co/CoO/NPCC/GCE. The obtained results indicate that NiCo/NiO-CoO/NPCC/GCE exhibits good electrocatalytic activity toward methanol oxidation, demonstrating a reasonable stability and durability. The enhanced performance can be attributed to the synergetic effect of the different components (NiCo, NiO-CoO, and carbon template). Also, in-situ preparation process of NiCo/NiO-CoO/NPCC/GCE is helpful to the formation of NiCo/NiO-CoO/GCE nanoparticles uniformly distributed in the carbon support, which avoids the growing and agglomeration metals/metal oxides into larger particles. In addition, carbon support enable electrons transport more rapidly and efficiently during the electrooxidation process. Moreover, the obtained nanocomposites with unique structure provide higher specific surface area, and more pores, which enlarge the electrode/electrolyte contact area and shorten the path length for ions transport to the active materials.

#### Acknowledgements

The authors gratefully acknowledge the support of this work by the Research Council and the Center of Excellence for Nanostructures of the Sharif University of Technology, Tehran.

#### References

- [1] J.B. Raoof, S.R. Hosseini, S. Rezaee, *Electrochim. Acta* 141 (2014) 340–348.
- [2] B. Abida, L. Chirchi, S. Baranton, T.W. Napporn, H. Kochkar, J.M. Léger, A. Ghorbel, *Appl. Catal. B: Environ.* 106 (2011) 609–615.
- [3] H.Y. Su, Y. Gorlin, I.C. Man, F. Calle-Vallejo, J.K. Nørskov, T.F. Jaramillo,

- J. Rossmeisl, *Phys. Chem. Chem. Phys.* 14 (2012) 14010–14022.
- [4] X. Tong, Y. Qin, X. Guo, O. Moutanabbir, X. Ao, E. Pippel, M. Knez, *Small* 8 (2012) 3390–3395.
- [5] S. Zafeiratos, T. Dintzer, D. Teschner, R. Blume, M. Hävecker, A. Knop-Gericke, R. Schlögl, *J. Catal.* 269 (2010) 309–317.
- [6] P. Pattanayak, N. Pramanik, P. Kumar, P.P. Kundu, *Int. J. Hydrogen Energy* 43 (2018) 11505–11519.
- [7] Y. Bai, J. Wu, X. Qiu, J. Xi, J. Wang, J. Li, L. Chen, *Appl. Catal. B: Environ.* 73 (2007) 144–149.
- [8] T. Liu, Y. Li, G. Quan, P. Dai, X. Yu, M. Wu, G. Li, *Matraga Rev. Do Programa Pós-graduação Em Let. Da Uerj* 139 (2015) 208–211.
- [9] N. Wang, P. Zhao, Q. Zhang, M. Yao, W. Hu, *Compos Part B-Eng.* 113 (2017) 144–151.
- [10] X. Liu, M. Park, M.G. Kim, S. Gupta, G. Wu, J. Cho, *Angew. Chem. Int. Ed.* 54 (2015) 9654–9658.
- [11] D. Wu, M. Wen, X. Lin, Q. Wu, C. Gu, H. Chen, *J. Mater. Chem. A Mater. Energy Sustain.* 4 (2016) 6595–6602.
- [12] Z. Peng, D. Jia, A.M. Al-Enizi, A.A. Elzatahry, G. Zheng, *Adv. Energy Mater.* 5 (2015) 1402031.
- [13] F. Zhang, N. Wang, L. Yang, M. Li, L. Huang, *Int. J. Hydrogen Energy* 39 (2014) 18688–18694.
- [14] Y. Wei, F. Yan, X. Tang, Y. Luo, M. Zhang, W. Wei, L. Chen, *ACS Appl. Mater. Interfaces* 7 (2015) 21703–21711.
- [15] J. Liang, H. Hu, H. Park, C. Xiao, S. Ding, U. Paik, X.W.D. Lou, *Synth. Lect. Energy Environ. Technol. Sci. Soc.* 8 (2015) 1707–1711.
- [16] X. Wang, L. Zhang, Z. Zhang, A. Yu, P. Wu, *Phys. Chem. Chem. Phys.* 18 (2016) 3893–3899.
- [17] M. Zhang, F. Yan, X. Tang, Q. Li, T. Wang, G. Cao, *J. Mater. Chem. A Mater. Energy Sustain.* 2 (2014) 5890–5897.
- [18] W.D. Zhang, J. Chen, L.C. Jiang, Y.X. Yu, J.Q. Zhang, *Microchim. Acta* 68 (2010) 259–265.
- [19] S. Shahrokhian, S. Rezaee, *Electroanalysis* 29 (2017) 2591–2601.
- [20] J.B. Wu, Z.G. Li, X.H. Huang, Y. Lin, *J. Power Sources* 224 (2013) 1–5.
- [21] P. Pachfule, X. Yang, Q.L. Zhu, N. Tsumori, T. Uchida, Q. Xu, *J. Mater. Chem. A Mater. Energy Sustain.* 5 (2017) 4835–4841.
- [22] L. Pan, T. Muhammad, L. Ma, Z.F. Huang, S. Wang, L. Wang, X. Zhang, *Appl. Catal. B: Environ.* 189 (2016) 181–191.
- [23] Y. Xu, Q. Li, H. Xue, H. Pang, *Coord. Chem. Rev.* 376 (2018) 292–318.
- [24] W.T. Koo, S. Yu, S.J. Choi, J.S. Jang, J.Y. Cheong, I.D. Kim, *ACS Appl. Mater. Interfaces* 9 (2017) 8201–8210.
- [25] Y. Jiao, J. Pei, D. Chen, C. Yan, Y. Hu, Q. Zhang, G. Chen, *J. Mater. Chem. A* 5 (2017) 1094–1102.
- [26] J.B. Raoof, S.R. Hosseini, R. Ojani, S. Mandegar, *Energy* 90 (2015) 1075–1081.
- [27] X. Xiao, Q. Li, X. Yuan, Y. Xu, M. Zheng, H. Pang, *Small Methods* (2018) 1800240.
- [28] Y. Shu, Y. Yan, J. Chen, Q. Xu, H. Pang, X. Hu, *ACS Appl. Mater. Interfaces* 9 (2017) 22342–22349.
- [29] Y.X. Xu, B. Li, S.S. Zheng, P. Wu, J. Zhang, H. Xue, H. Pang, *J. Mater. Chem. A Mater. Energy Sustain.* 6 (2018) 22070–22076.
- [30] I. Ali Khan, A. Badshah, N. Haider, S. Ullah, D.H. Anjum, M.A. Nadeem, *J. Solid State Electrochem.* 18 (2014) 1545–1555.
- [31] Y. Jiao, J. Pei, D. Chen, C. Yan, Y. Hu, Q. Zhang, G. Chen, *J. Mater. Chem. A Mater. Energy Sustain.* 5 (2017) 1094–1102.
- [32] J. Yang, C. Zheng, P. Xiong, Y. Li, M. Wei, *J. Mater. Chem. A Mater. Energy Sustain.* 2 (2014) 19005–19010.
- [33] X. Hu, H. Hu, C. Li, T. Li, X. Lou, Q. Chen, B. Hu, *J. Solid State Chem.* 242 (2016) 71–76.
- [34] L. Chu, M. Li, X. Li, Y. Wang, Z. Wan, S. Dou, B. Jiang, *RSC Adv.* 54 (2015) 9765–9770.
- [35] C. Teng, J. He, L. Zhu, L. Ren, J. Chen, M. Hong, Y. Wang, *Nanoscale Res. Lett.* 10 (2015) 384.
- [36] Y.C. Wang, W.B. Li, L. Zhao, B.Q. Xu, *Phys. Chem. Chem. Phys.* 18 (2016) 17941–17948.
- [37] X. Lou, H. Hu, C. Li, X. Hu, T. Li, M. Shen, B. Hu, *RSC Adv.* 6 (2016) 86126–86130.
- [38] H. Hosseini, S. Shahrokhian, *Chem. Eng. J.* 341 (2018) 10–26.
- [39] Z. Wu, J. Wang, L. Han, R. Lin, H. Liu, H.L. Xin, D. Wang, *Nanoscale* 8 (2016) 4681–4687.
- [40] H. Hosseini, S. Shahrokhian, *Appl. Mater. Today* 10 (2018) 72–85.
- [41] P. Zhang, R. Wang, M. He, J. Lang, S. Xu, X. Yan, *Adv. Funct. Mater.* 26 (2016) 1354–1364.
- [42] Y. Xu, W. Tu, B. Zhang, S. Yin, Y. Huang, M. Kraft, R. Xu, *Adv. Mater.* 29 (2017) 1605957.
- [43] J.W. Lee, T. Ahn, J.H. Kim, J.M. Ko, J.D. Kim, *Electrochim. Acta* 56 (2011) 4849–4857.
- [44] D. Wang, W. Ni, H. Pang, Q. Lu, Z. Huang, J. Zhao, *Electrochim. Acta* 55 (2010) 6830–6835.
- [45] Y. Yan, P. Gu, S. Zheng, M. Zheng, H. Pang, H. Xue, *J. Mater. Chem. A Mater. Energy Sustain.* 4 (2016) 19078–19085.
- [46] D.O. Miles, D. Jiang, A.D. Burrows, J.E. Halls, F. Marken, *Electrochem. commun.* 27 (2013) 9–13.
- [47] Y.Y. Tong, C.D. Gu, J.L. Zhang, H. Tang, X.L. Wang, J.P. Tu, *Int. J. Hydrogen Energy* 41 (2016) 6342–6352.
- [48] N.A. Barakat, M.A. Abdelkareem, M. El-Newehy, H.Y. Kim, *Nanoscale Res. Lett.* 8 (2013) 402.
- [49] W. Wang, R. Li, X. Hua, R. Zhang, *Electrochim. Acta* 163 (2015) 48–56.
- [50] Y.Y. Tong, C.D. Gu, J.L. Zhang, H. Tang, Y. Li, X.L. Wang, J.P. Tu, *Electrochim. Acta* 187 (2016) 11–19.
- [51] X. Cui, W. Guo, M. Zhou, Y. Yang, Y. Li, P. Xiao, X. Zhang, *ACS Appl. Mater. Interfaces* 7 (2014) 493–503.
- [52] J.B. Wu, Z.G. Li, X.H. Huang, Y. Lin, *J. Power Sources* 224 (2013) 1–5.
- [53] R.H. Tammam, A.M. Fekry, M.M. Saleh, *Int. J. Hydrogen Energy* 40 (2015) 275–283.
- [54] R. Ding, L. Qi, M. Jia, H. Wang, *J. Power Sources* 251 (2014) 287–295.
- [55] R. Ding, L. Qi, M. Jia, H. Wang, *Electrochim. Acta* 113 (2013) 290–301.
- [56] J.B. Raoof, S.R. Hosseini, S. Rezaee, *J. Mol. Liq.* 200 (2014) 196–204.
- [57] M. Yang, F. Lv, Z. Wang, Y. Xiong, M. Li, W. Wang, Z. Lu, *RSC Adv.* 5 (2015) 31725–31731.
- [58] S. Rezaee, S. Shahrokhian, M.K. Amini, *J. Phys. Chem. C* 122 (2018) 9783–9794.